Separation of Empty and Water-Filled Single-Wall Carbon Nanotubes

Jeffrey A. Fagan,[†,*] Ji Yeon Huh,[†,¶] Jeffrey R. Simpson,[‡] Jeffrey L. Blackburn,[§] Josh M. Holt,[§] Brian A. Larsen,[§] and Angela R. Hight Walker[⊥]

[†]Polymers Division, National Institute of Standards and Technology, Gaithersburg Maryland 20899, United States, [‡]Towson University, Towson Maryland 21252, United States, [§]National Renewable Energy Laboratory, Golden, Colorado 80401, United States, and [⊥]Optical Technology Division, National Institute of Standards and Technology, Gaithersburg Maryland 20899, United States. [¶] Present address: DuPont Central Research & Development, Wilmington, Delaware, 19880—0304.

ABSTRACT The separation of empty and water-filled laser ablation and electric arc synthesized nanotubes is reported. Centrifugation of these large-diameter nanotubes dispersed with sodium deoxycholate using specific conditions produces isolated bands of empty and water-filled nanotubes without significant diameter selection. This separation is shown to be consistent across multiple nanotube populations dispersed from different source soots. Detailed spectroscopic characterization of the resulting empty and filled fractions reveals that water filling leads to systematic changes to the optical and vibrational properties. Furthermore, sequential separation of the resolved fractions using cosurfactants and density gradient ultracentrifugation reveals that water filling strongly influences the optimal conditions for metallic and semiconducting separation.

KEYWORDS: nanotube · SWCNT · centrifugation · separation · deoxycholate · empty · water-filled

The necessity for the separation of single-wall carbon nanotube (SWCNT) populations to achieve desired properties is a major technical barrier for the development of SWCNT based applications and has been the focus of significant academic and industrial research.[1,2] Recent advances include the separation of SWCNT populations by diameter through density differences,[3−5] separation of metallic and semiconducting nanotubes through the use of cosurfactants[4,6,7] and selective salt effects,[8] separation by chiral angle,[9,10] separation by handedness,[5,11,12] and the specific selection of single chiralities in anionic exchange chromatography[13] using specific DNA sequences.[14] The driving factor in each of these separations is hypothesized to be the specific interactions of the dispersant with the outer nanotube surface.[15] However, for damaged nanotubes, or nanotubes without an endcap on both ends, it is likely that the interior of the nanotube will be accessible to the environment, and potentially filled by the solvent,[16] ions or other molecules,[17−19] or dispersed nanoparticles.[20] Whether the nanotube is empty or filled simply with water has been theoretically identified as significantly affecting the density of the dispersed nanotubes[21−23] and thus will also affect nanotube separation techniques exploiting buoyancy differences.

Previous results in the literature by Wenseleers *et al.*[24] and Cambré *et al.*[25] have also established the substantial effects of water-filling on experimentally measurable nanotube properties. Using resonant Raman scattering, they demonstrated that the radial breathing modes (RBMs) of small-diameter nanotubes filled with water harden in a diameter dependent manner and they reported shifts in the optical transition energies with the water-filling. Moreover, they found that most nanotubes were opened after dispersion processing,[24] a finding that has significant importance to both the achievable properties of nanotubes in solution and for the separation of nanotubes through centrifugation-based processing.[21−23] This finding also explains why the separation of empty and water-filled nanotubes has not been previously addressed in the literature;[26,27] in many experiments such as density gradient ultracentrifugation (DGU) for chirality separation, the small amount of empty nanotubes would likely have been observed as a creamed layer not exhibiting chirality separation and discarded.

In this contribution, we report a facile method for separating water-filled and empty (end-capped) nanotubes from an initial mixture using a rate zonal centrifugation method and the resulting spectroscopic properties of the distinct populations. In particular, results are shown demonstrating separation for laser ablation and electric arc synthesis produced nanotubes with diameters ranging from 1.2 to 1.5 nm using deoxycholate (DOC) surfactant[28,29] based on the absence or presence of liquid in the interior cavity. Isolation of these populations was achieved from multiple SWCNT populations obtained from

* Address correspondence to jeffrey.fagan@nist.gov.

Received for review February 3, 2011 and accepted April 11, 2011.

Published online April 11, 2011
10.1021/nn200458t

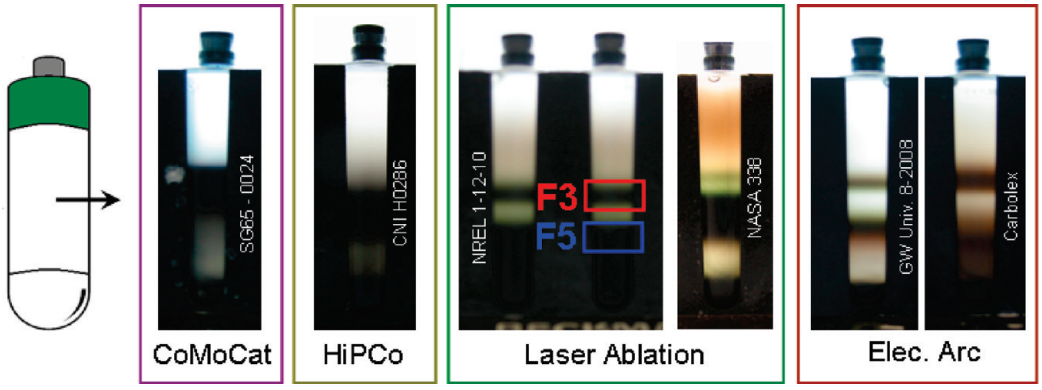

Figure 1. Schematic of experimental setup and pictures of the resulting distribution of SWCNTs after 1 h of centrifugation at 6800 rad/s for six sources of nanotubes from four different production methods. The average diameter of the SWCNTs in the dispersion increases left to right. Consistent band formation was observed after separation for the laser ablation and electric arc produced SWCNTs. Upper dark bands (fraction 3, F3) contain empty nanotubes of the same chiralities as the water-filled SWCNTs that separate into the lower band (fraction 5, F5). Different relative amounts of the empty and water-filled nanotubes are visible from the various source soots. Two separated tubes of the NREL SWCNTs are shown to demonstrate the tube-to-tube consistency. Note that in all of the tubes shown, a layer of density medium (not visible due to the holder) separates the bottommost nanotube layer from the bottom of the tube.

several independent synthesis sources. The separated populations are demonstrated to have significantly different optical resonance energies, radial breathing mode locations, and fluorescence efficiencies, as well as different optimal conditions for metallic and semiconducting separation. As previously noted,[25] the spectroscopic signatures of typically produced samples are dominated by the water-filled nanotubes, which are shown to make up the bulk of a mixture under typical sonication conditions. This implies that many of the reported optical studies of SWCNT samples have primarily probed the spectroscopic properties of water-filled SWCNTs, underscoring the importance of the method developed here for separation of the empty, end-capped SWCNTs from mixed populations.

RESULTS

In the absence of convection in the fluid, the motion of dispersed SWCNTs under the application of a centripetal acceleration depends on the size and shape of the particle, as well as its buoyancy. Controlling the individual motion of the dispersed particles through these parameters is the basis for density gradient ultracentrifugation and rate zonal centrifugal separations, the difference being in that density gradient separations imply an exploitation of equilibrium properties, and rate zonal separations[30,31] rely on differences in transient motion. A vertical rotor[32,33] was chosen for the experiments described here since separation by the buoyant density difference was primarily desired. This type of rotor is particularly useful for isopycnic separation of nonpelleting materials[34] due to the short path length particles must travel to redistribute within the tube, and the large applicable acceleration that can be produced. It is also beneficial in that the ratio of the loading volume of material to be separated to the race layer fluid volume can be much higher in the vertical rotor than in a swinging bucket geometry. To provide a tunable liquid density distribution, a common density modifying liquid, iodixanol, was added to some layers in the centrifuge tube.

The initial goal of these experiments was to improve the separation of (6,5) nanotubes from a cobalt–molybdenum–catalyst synthesis method (CoMoCat) sample, and thus the centrifuge tube was loaded in three sections, with a dense bottom layer, a large race layer at a density approximating that of the (6,5) SWCNTs, and a top layer in which the nanotubes were introduced. The separation was then run for 1 h at 6810 rad/s; the acceleration in the liquid under these conditions is equivalent to approximately 400 000 times standard gravitational acceleration (g = 9.81 m/s^2). A diagram of the setup is included in Figure 1; details are included in the Methods section. Because the separation is neither wholly rate dependent nor an equilibrium phenomenon due to the sedimentation of the density gradient medium, SWCNT samples from multiple synthesis sources were processed with an eye toward diameter selection in the different populations.

To vary the average diameter of the nanotubes in the experiment we used nanotube soots generated by different techniques that yield increasing average diameters ($\langle D \rangle$). In order of average diameter, the production techniques were as follows: the CoMoCat method, $\langle D \rangle \approx$ 0.8 nm; the high pressure CO conversion (HiPCO) process, $\langle D \rangle \approx$ 1.0 nm; laser ablation synthesis, $\langle D \rangle \approx$ 1.3 nm; and electric arc (EA) synthesis, $\langle D \rangle \approx$ 1.5 nm. SWCNT samples were acquired from suppliers including Southwest Nanotechnologies, Carbon Nanotechnologies Inc. (CNI), NASA Johnson Space Center, the National Renewable Energy Lab (NREL), Rochester Institute of Technology, Carbolex Inc., and George Washington University (GWU). Photographs of

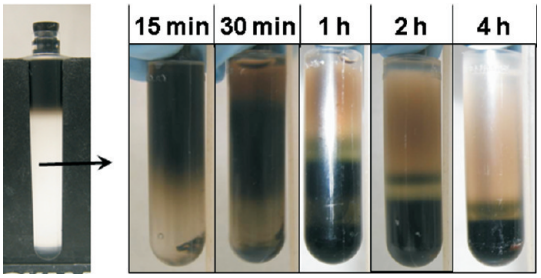

Figure 2. Sequential photographs of the separation of the empty and water-filled nanotubes from a laser ablation source soot in the vertical rotor. Note the progressive motion of bands through the liquid column, and the distinct separation of the upper and lower nanotube bands. Minor changes to the bottom layer density and/or the total time can be used to optimize the experiment for separation of either the empty or the water-filled nanotube band.

the results of the separation are shown in Figure 1 for SWCNT dispersions from several production methods.

Separation of the CoMoCat SG65 sample in the vertical rotor experiment is the most consistent with previously reported separations using DGU. A single main band of nanotubes progresses through the solution with time, with the most buoyant chiralities such as the (6,5) enriched at the upper clarified interface (data not shown) due to the lesser buoyancy difference to the density gradient medium. Additionally, and in all experiments, a fraction of the parent nanotube dispersion rapidly sediments to near, but suspended above, the bottom of the tube. Diameter separation in the upper band is less pronounced in this experiment using DOC than for prior work that used sodium cholate (SC) as the surfactant for reasons beyond the scope of this contribution, but that are well described elsewhere.[15]

For the larger diameter samples however, instead of a continuous diameter separation as seen in the CoMoCat synthesis nanotubes, the separation results in the isolation of two bands within the race layer of the centrifuge tube. These comprise empty, low density, nanotubes in the top band (F3 in Figure 1), and water-filled (F5 in Figure 1), with a greater density, nanotubes in the bottom band (*vide infra*). Halting the centrifugation at shorter/longer times demonstrates that the motion of the nanotube bands through the medium is progressive and that bulk convection or other artifacts are not the source of the banding in the larger diameter samples. The progressive nature of the separation is demonstrated in Figure 2, in which photographs show the separation of laser ablation synthesized nanotubes at increasing time points.

A comparison of the location of the separated bands with increasing average nanotube diameter in Figure 1, shows two notable observations: first, the separation distance between the F3 and F5 bands increases with increasing nanotube diameter, and, second, the lower band progresses further down the liquid column with increasing nanotube diameter. Both of these observations are consistent with the changes in the average density predicted for empty and water-filled nanotubes with increasing diameter.[23]

We have also noted that the isolation of the two distinct bands in the separation is robust and varies only slightly with temperature (4−20 °C), DOC content (1%−2% in the race layer), and the bottom layer density (15%−18% (mass/volume) iodixanol). However, minor changes to the bottom layer density and/or the total time can be used to optimize the experiment for separation of either the empty, or the water-filled, nanotube band. Optimization is most important for the isolation of the empty tubes from the water-filled HiPCO source SWCNTs, due to the small difference in density between the two populations. The details of the HiPCO separation and characterization will be expanded upon in a later communication.

In this contribution, we primarily use fraction F3 and fraction F5, labeled in Figure 1, from the NREL synthesized laser ablation nanotubes to verify the empty and water-filled hypothesis and to explore the consequences of the filling on the optical properties of the nanotubes. The source layers of these fractions are denoted in Figure 1. The remaining volume of the separated material from the laser ablation and electric arc synthesis methods appears to contain fullerenes, visible as the top brownish layer above the upper nanotube band, less optically active nanotubes, present in the fractions below F5, and a small amount of non-nanotube material and bundles that comprises the sediment. F4, which is the fraction collected from in between the two primary bands, displays optical properties primarily similar to F3, but with contamination by F5 material. The absolute amount of material in F4 is significantly lower than in either F3 or F5, visible in Figure 1, and probably contains material due to a combination of effects such as the finite thickness of the initial nanotube layer, nanotube−nanotube interactions, and the length dependence of mobility for a rod. Some shift in the diameter distribution toward larger diameters is also visible for the fractions below F5, but is relatively minor. It is also possible that given a higher position resolution in fractionation, or *in situ* measurement of the chirality distribution,[5] that small shifts in the chirality distribution across the collected bands may be measurable. However attempts at finer separation of the fractions by collecting and separating them again has indicated that this is a minor effect that would not alter the interpretation of the data. That this effect is small is not surprising, given the small density differences between the SWCNTs compared to their difference from the medium, and the significant thickness of the injection band in the experiment. Full absorbance spectra for all separated fractions are reported in the Supporting Information.

To allow for a thorough examination of the isolated bands, the separation was performed a minimum of 16

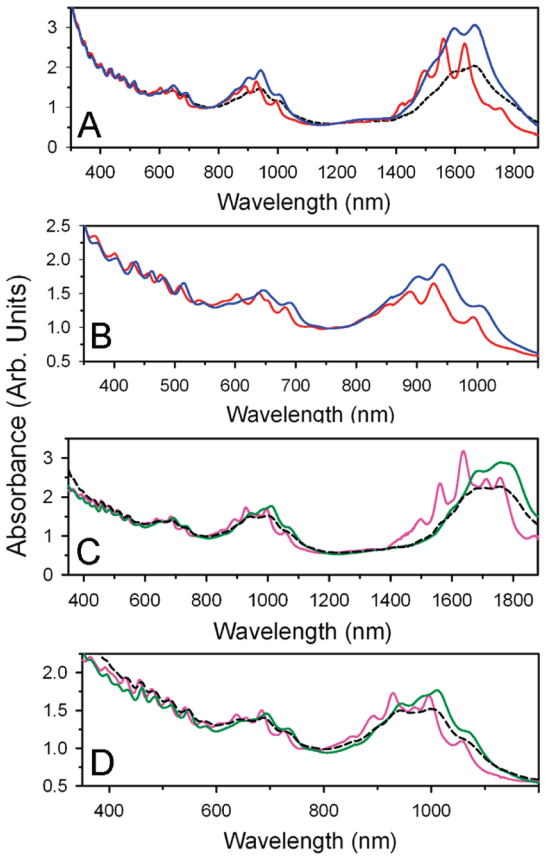

Figure 3. (A) Absorbance spectra of the two bands (red, F3; blue, F5) separated from the NREL-produced laser ablation parent SWCNT dispersion (black, short dashes) in Figure 1. Absorbance features due to the semiconducting SWCNTs (S_{11}, 1800−1400 nm; S_{22}, 1100−800 nm; and S_{33}, 550−400 nm) and metallic SWCNTs (M_{11}, 750−550 nm) are clearly visible in both fractions. (B) Close up of panel A to demonstrate that the clear interdigitation of the peak features is observable in all transition band regions, although the diameter distributions, roughly defined by the wavelength range of the transitions, are approximately the same. (C) Absorbance spectra of the two bands (pink, top; green, lower) separated from the GWU electric arc produced parent SWCNT dispersion (black dashes) in Figure 1. (D) Close up of panel C to demonstrate that the clear interdigitation of the peak features is observable in all transition band regions for the electric arc SWCNTs. Note that the wavelength range shown is wider in panel D than in panel B as the optical transitions occur at longer wavelengths.

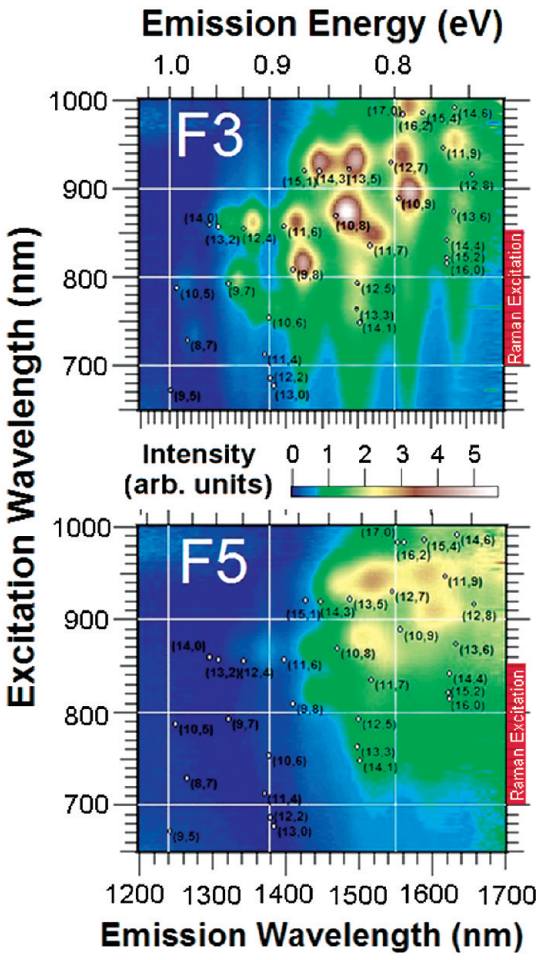

Figure 4. NIR fluorescence for F3 (top) and F5 (bottom) of the separated NREL laser ablation SWCNTs. Clear peak features exist in both fractions. The locations of assigned peak features measured using SWCNTs dispersed in SDS[40] are noted with white dots. In both fractions, peaks corresponding to the same assigned locations for the SDS-dispersed SWCNTs are visible. There are no expected peaks missing in the F3 sample. The location of the peaks in F5 however are red-shifted a greater amount in both excitation and emission wavelength, and of lower intensity, than the peaks in F3. It is likely that some chiralities present in the sample are excited by or emit at longer wavelengths than those experimentally measured; negligible NIR fluorescence emission was measured below 1200 nm.

times for each of the laser ablation and electric arc SWCNT sources. For the primary fractions reported in this paper, roughly 50 centrifuge tubes of the NREL laser ablation source were spun in the rotor and the like fractions combined. The repetition generated roughly 25 mL of sample of each fraction, from which the density gradient medium was removed and the absolute concentration of the SWCNTs was increased using a forced dialysis cell prior to characterization.

The distinctiveness of the optical properties from the two bands after mixing the roughly 50 fractions speaks to the high selectivity and reproducibility of the facile separation. The absorbance (Figure 3), NIR fluorescence (Figure 4), and Raman scattering (Figure 5) of the separated layers from the laser ablation (NREL) sample demonstrate that the two distinct bands in the middle of the tube contain SWCNTs of equivalent diameters. The details of these characterizations are addressed in order.

Figure 3 displays absorbance spectra of the separated bands collected from the NREL laser ablation and GWU electric arc synthesized materials. Clear differences in the peak locations and sharpness of the absorbance features (for F3 relative to F5) are visible for the all of the excitonic transitions, despite similar ranges for the transition energies that roughly represent the diameter distribution. Distinct sets of peak features belonging to the two bands occur in all laser ablation and electric arc synthesized SWCNTs

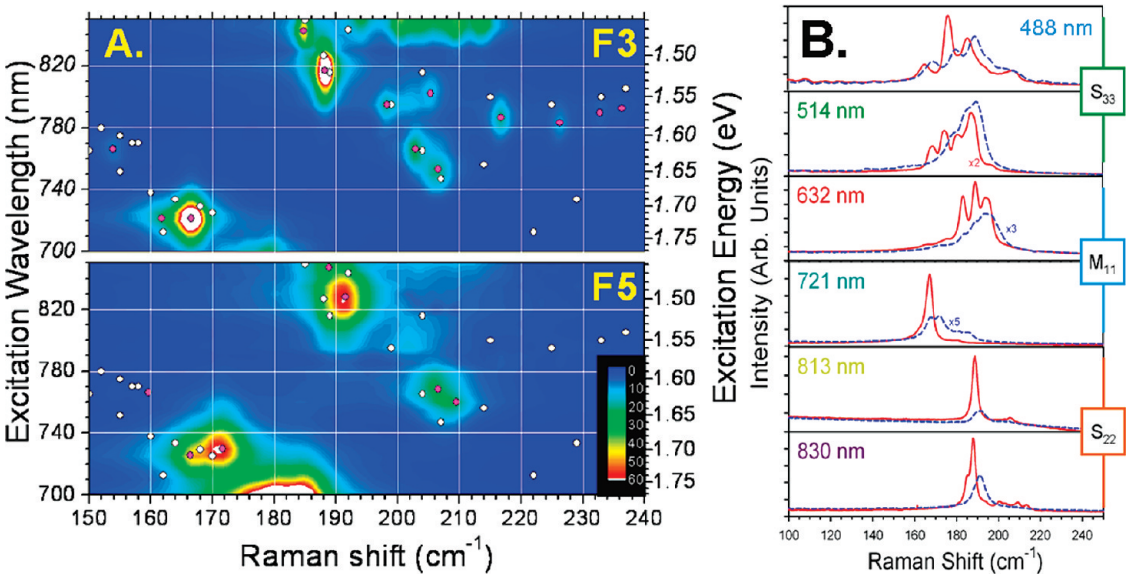

Figure 5. (A) Resonant Raman scattering in the RBM region of F3 and F5 separated from the NREL laser ablation SWCNTs for excitation wavelengths from 700 to 850 nm. (B) Single line scans of Raman scattering for excitation at noted wavelengths. In both panels, the RBM modes (peak features) of the two separated fractions have distinctly different shifts, with the F5 peaks hardened and red-shifted in peak excitation energy. This distinctiveness in the locations of the Raman shifts is visible for both semiconducting SWCNTs, measured with excitation wavelengths above 750 nm (S_{22} excitation), and for the metallic SWCNTs (Figure 5A, M_{11} excitation). Note, although peaks are highlighted by pink dots, these positions are marked to highlight lower intensity features and do not represent previously assigned values from the literature. An empirical set of RBM assignments are noted on the figure (white points).[47]

separated (see Supporting Information), although the fraction of the initial material that distributes into the empty and water-filled bands varies with the source soot and parameters such as the sonication time. An additional important observation (show in the Supporting Information) is that the absorbance peak features in the F3 bands, and separately for the F5 bands, are located at the same wavelength positions regardless of the source soot or the synthesis method (for the overlapping parts of the diameter distribution).

The data in Figure 3 also indicates that the diameter distribution is the same or similar in the two bands, which eliminates the possibility that the band separation and spectral shifts are due to intraspecies density differences caused by enantiomer effects, as those differences are much smaller than the interspecies differences.[5,12] Additionally, the observation that metallic optical transitions demonstrate the same shifts, despite the presence of achiral metallic species, is another indicator that enatiomeric effects are not a significant factor in this separation.

Scaling the spectra pairs from each of the NREL laser ablation and GWU electric arc samples to an absorbance value of one at 770 nm, the absorbance in the π-plasmon region can be seen to be nearly overlapping in magnitude in the F3 and F5 fractions. Although both bands have larger scaled peak absorbance than the parent dispersion due to the removal of impurities in the centrifugation process, the lower band (F5) exhibits measurably larger integrated absorbance in the electronic transitions than F3. This observation that the peak size increases in the F5 band from the parent sample is another in a series of results that strongly imply that the F5 band is not an aggregated state of the F3 band, and that the measured shifts in transition energies are instead a function of water filling.

It bears repeating that the shifts in the locations of the optical transitions for F3 relative to F5 are observed for all of the transitions visible in Figure 3—S_{11}, S_{22}, S_{33}, and M_{11} transitions—which results in the "interdigitated" appearance of the transition envelopes, as shown in Figure 3b. That the location of the optical transitions should shift with water filling of the SWCNT core is not surprising, and is in line with the effect of water filling reported by Wenseleers *et al.*[24] and Cambré *et al.*[25] Similar to previously demonstrated effects of the local external dielectric constant and degree of surface coverage on the SWCNT optical properties,[35−37] modification of the *internal* dielectric constant *via* accessibility of the inner surface is also expected to change the optical properties. Red-shifted features in the water-filled SWCNTs, with a higher internal dielectric constant relative to the empty SWCNTs is moreover consistent with the previously reported effects of a higher dielectric constant on the exterior of the dispersed nanotubes.

Semiconducting SWCNTs exhibit distinct fluorescence in the near-infrared (NIR)[38,39] that can be used to assign the presence or absence of a nanotube in a population, as well as to demonstrate local dielectric affects on specific SWCNT transition energies with more precision than the absorbance method. Figure 4

shows the NIR fluorescence maps for the two samples in Figure 3. Sharp, well-resolved peaks are visible in fraction 3, corresponding to luminescence features from both minor and major SWCNT species. In contrast, the peak features are red-shifted in both excitation and emission energies and of lower intensity in the F5 band.

An interesting observation is that the F3 sample is significantly brighter (~2×) than the F5 sample when both are diluted to equivalent concentrations as shown in Figure 3, despite the greater magnitude of the peak optical transitions measured in the absorbance spectra for the F5 sample. Also of note, is that peaks previously assigned to all of the chiral species expected to be present in the excitation range[40] are visible in both fractions, although shifted from the reported peak positions in SDS dispersion due to the difference in the local dielectric environment. The presence of all the chiralities is particularly clear in the F3 sample. Our interpretation is that the data show that common SWCNT species have different effective quantum yields in the two fractions due to water filling, and that the shifted peaks are not indicative of chirality separation between the two samples. The NIR fluorescence quantum yield has previously been shown to be sensitive to the local external environment surrounding the nanotubes.[37,41,42] However, in both samples shown in Figure 4, the bulk environment is nearly identical, as ensured by thorough diafiltration and dilution by the same D_2O−surfactant solution for the experiment. We believe that this is instead the first demonstration of the effect of water filling on the fluorescence of the SWCNTs. Importantly, the NIR fluorescence map of the same SWCNT parent sample dispersed with DOC (Supporting Information) and not subjected to separation closely approximates, excepting overall intensity, the map of the water-filled SWCNTs (F5) extracted by the separation. This indicates that the dominant fraction of SWCNTs in a typically dispersed sample are water-filled. Thus, some of the variation in previous literature reports for quantum yields may reflect the effects of uncontrolled solvent intrusion into the measured nanotubes, in addition to the effects of defects in different nanotube batches, and differences in the isolation of the SWCNTs from the solvent environment by the dispersant molecule.[37,43] Additional fluorescence data is reported in the Supporting Information.

Resonant Raman scattering is another technique that can directly determine the population of chiralities within a nanotube sample and is often used for nanotube dispersions. In particular, the radial breathing mode (RBM), a resonant feature that is related to the radial expansion and contraction of the nanotube, is often used to assign[44−46] the presence or absence of specific nanotubes in a dispersed population. As we will demonstrate, the implications of water-filling to the assignment of species in a population are significant. Wenseleers *et al.*[24] and Cambré *et al.*[25] previously demonstrated that the RBM mode of a nanotube is hardened (requires more energy) when the nanotubes are water-filled, primarily for smaller diameter nanotubes. Hardening of the RBM modes has also been reported for laser ablation SWCNTs filled with β-carotene.[19] In Figure 5A, the Raman scattering in the RBM region is reported for the F3 and F5 samples for the excitation range from 695 to 855 nm. Over this excitation window, a portion of the chiralities in the sample are in resonance with either their metallic optical transitions, M_{11}, or their semiconducting, S_{22}, optical transitions for the laser ablation diameter nanotubes.[47] Raman measurements for individual excitation lines extending beyond the 700−855 nm window are shown in Figure 5B. Additional Raman data covering more single wavelength excitation scans, including additional excitation of the M_{11} and S_{33} optical transitions, and the evolution of the Raman spectra with the applied processing, are reported in the Supporting Information.

The distinct separation of the RBM modes in the two populations visible in both the contour plots and line scans in Figure 4 is striking. For both M_{11} and S_{22} excitation there are clear shifts in the RBM location (~4 cm^{-1}) and peak excitation wavelength (~5 nm). These shifts are large enough that without thorough characterization, and due to the limited data for RBM locations in many surfactants,[46] the shifted features could easily lead to mistaken assignments regarding the presence of different chiralities in the two samples. With a wide excitation window, and referencing to the empirical RBM locations fit to sodium dodecylbezenesulfonate (SDBS) data,[47] it is clear that the primary RBM peaks in the two fractions are, by elimination of other possibilities, for the same chirality nanotubes.

A closer look at the effects of the water-filling on the Raman is shown in Figure 6a and 6b. In Figure 6a, the excitation cross sections are compared for two of the identified chirality nanotubes. Plotting the scaled intensity of the Raman scattering at the peak RBM wavenumber positions, it is clear that the F5 fraction resonance is red-shifted and broader than the same species nanotube in the F3 fraction. Collecting values for the degree of shift measured with the water-filling for all the measured SWCNTs in Figure 6b, we can compare to the degree of hardening observed with water-filling in smaller diameter nanotubes.[25] In general, the values for hardening measured for the laser ablation and electric arc synthesized nanotubes in this contribution are consistent with those reported in the literature[28] and continue a trend of increasing hardening for larger diameter nanotubes.

Additional Raman scattering measurements covering the D, G, and G′ (Supporting Information) reveal that for both populations the *D*/*G* ratio is <1/75 and 1/100 at 514 nm excitation for F3 and F5, respectively.

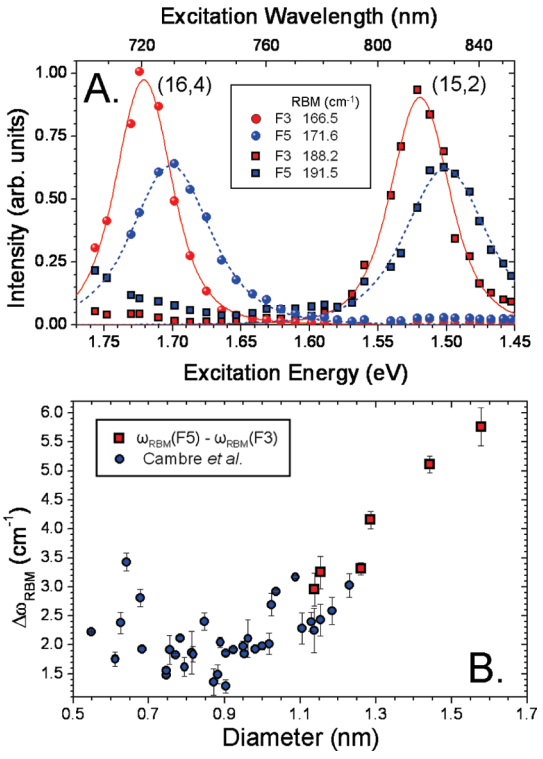

Figure 6. (A) Comparison of the excitation slices for two different chirality nanotubes with water-filling; squares are for data assigned to the (15,2) chirality, circles are for data assigned to the (16,4) chirality. In both instances, F3 data are represented by red symbols, and the fits to the data are represented with solid lines. F5 data are represented by blue symbols, and the fits to the data are represented by the dashed curves. For both chirality nanotubes, the excitation resonance is red-shifted for the water-filled SWCNTs, and the fwhm values are broader. (B) Comparison of the RBM frequency shift upon filling with endohedral water as measured for specific chiralities in this work along with those values reported by Cambré *et al.*[25] The values in this work extend the plot to include larger diameter nanotubes.

Defects are thus not an apparent contributor to the difference in measured properties. Using the relation ω_{RBM} (cm^{-1}) = (227/d (nm))((1 + 0.05786d^2)$^{1/2}$),[48] the range of observed diameters in the two laser ablation synthesis fractions is approximately 1.1−1.4 nm. Taken together, the absorbance, fluorescence, and Raman scattering data indicate that the two bands contain near-identical populations of chiralities, with the properties of the populations split by the environmental effect of the condition of the tube interior.

Despite the direct inference from the optical data that the chirality populations are similar in the two bands, and that it is water-filling that accounts for the differences, additional experiments were conducted to verify the hypothesis and to eliminate alternate mechanisms. From a broad perspective, multiple phenomena could be responsible for shifting peak locations in the optical data. These include bundling of the nanotubes, differential adsorption of surfactant on nanotubes of different chiral handedness, and populations with different structures of adsorbed surfactant.

Differences in bundling can be excluded due to several observations beyond those extrapolated from the optical data. The first observation, discussed in more detail below, is that the red-shifted F5 fraction is the sample that is easily separated into metallic and semiconducting SWCNT fractions, and that the peak locations are identical after the separation in the daughter fractions. It is not tenable that mixed bundles of nanotubes would disaggregate, separate, and rebundle while exhibiting consistent optical transition locations. A second observation is that the location of the optical transitions is invariant in time in the two fractions, whereas shifts in the positions of the transitions would be expected with dilution or concentration of samples if a bundling/debundling mechanism was active in the samples. Lastly the position of the bands in the density column after separation indicates a density much lower than that observed for bundled nanotubes.[49]

The possibility of chirality or chiral handedness specific adsorption of the deoxycholate surfactant onto the nanotubes resulting in a buoyancy difference was also investigated. To explore this possibility, laser ablation nanotubes (NREL) were dispersed in surfactants other than DOC including $(GT)_{15}$ ssDNA, SDBS, and SC in the same manner as the dispersion in DOC. Separation in the vertical rotor at the same conditions was then performed; layers included the test surfactant and iodixanol. For both the DNA and the SDBS experiments the iodixanol content of the two bottom layers was however increased to 15% and 20% for the SDBS and 18% and 20% for the DNA to account for the higher density of the nanotubes in those dispersions. Photographs and spectra of these separations are shown in the Supporting Information (Figure 13S).

In SDBS a set of bands similar to those seen in the DOC dispersed separation were obtained after the separation. Although, the top band had a much lower concentration (∼1/11) after separation of the SDBS dispersion, the two bands for the SWCNTs dispersed in SDBS displayed optical features with relative shifts (for F3 relative to F5) similar to those observed for the DOC dispersed nanotubes. The features in both spectra are blue-shifted relative to the DOC dispersed separated fractions due to the different dielectric environment. SC dispersed SWCNTs were also found to form a similar upper band to the DOC-dispersed SWCNTs, also with similar optical feature shifts relative to the lower band, although at a concentration approximately one-fifth of the DOC upper band. No band separation was found for DNA-dispersed nanotubes at the conditions of the DOC−SWCNT separation, or with a greater density medium concentration, 18% in the race layer. We attribute this to the greater density of DNA−SWCNTs compared to surfactant wrapped SWCNTs, which caused complete sedimentation to the bottom. However, if the DNA−SWCNTs were layered on top of race layers containing DOC, the

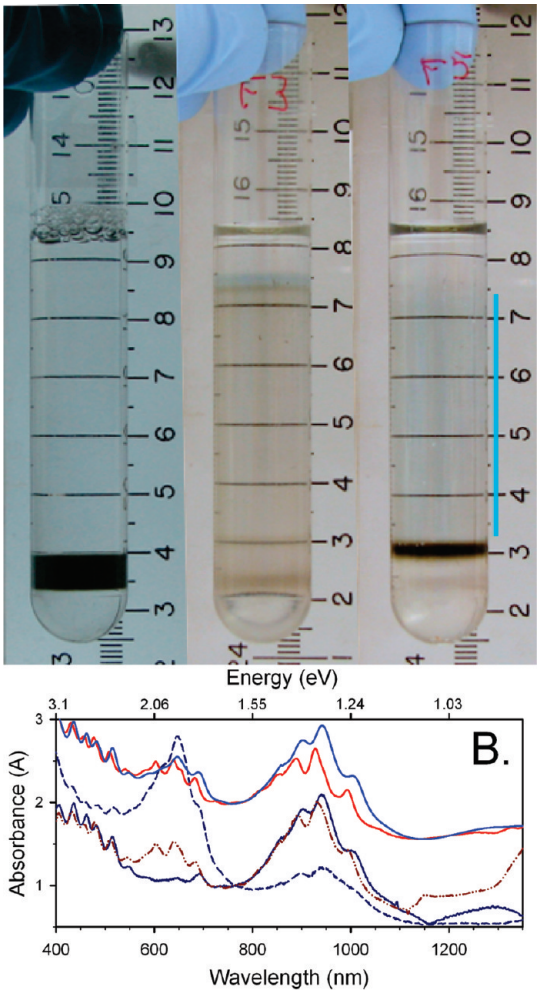

Figure 7. (A) Photographs of a metallic-semiconducting SWCNT separation using the cosurfactant strategy separation for NREL F3 and F5. Left to right, the photographs show the initial liquid layering, and the separated F3 and F5 populations after centrifugation. These pictures were taken for an iodixanol content of 30% in the layer above the nanotubes, and the F3 and F5 fractions were separated in the same centrifugation. The separation of the metallic and semiconducting SWCNTs in the F5 sample is near-ideal, with little cross contamination of the semiconducting (thin, brown band) and the metallic nanotubes (the area highlighted by the blue line was collected as a single fraction). Visibly different, the separation of the F3 sample has a broad central band comprising a mixed population of semiconducting and metallic nanotubes. (B) Scaled absorbance spectra of the parent F3 and F5 fractions (red and blue lines, respectively) and of the metallic (dark blue dashes) and semiconducting (dark blue line) fractions resulting from the separation of the water-filled F5 sample in the experiment shown in the photographs. The parent spectra are offset for clarity. The broad central band of the F3 separation is the dark red dash−dot−dot curve; substantially less change in the population is observed in the separation of the F3 parent than is for the separation of the F5 sample.

DNA was exchanged for DOC on the surface of the nanotube during the experiment, and a small upper band was again observed. These results directly support the empty and water-filled SWCNT hypothesis, as it is unlikely that shifts in the optical transitions due to selective absorption as a function of chiral angle or chiral handedness would be a common feature across different chiral and achiral surfactants.

Dilution of the DOC dispersed and separated F3 and F5 fractions into SDBS solutions were used to address the possibility that the optical shifts are related to differences in the uniformity of the surfactant packing. In both cases the locations of the optical transition features shifted a similar amount with the replacement of the dispersant. Fluorescence data for the F3 and F5 fractions diluted into SDBS are shown in the Supporting Information.

We can also compare the motion of the nanotube bands through the liquid to each other in a simple manner assuming that diffusion is negligible compared to the ballistic motion of the nanotubes through the liquid. In this case, the density difference between the two bands, $(\Delta\rho_2 - \Delta\rho_1)$, can be estimated from the experimental separation of the two bands after the hour run, ~5 mm, using eq 1,[30]

$$\text{separation} = (\Delta\rho_2 - \Delta\rho_1)\left(\frac{r^2 G t}{6\mu}\right)\left(\frac{2\gamma^4 + 0.614\gamma^3 + 0.544\gamma^2 - 0.136}{\gamma^3 + 0.614\gamma^2 + 0.638\gamma + 0.135}\right) \quad (1)$$

in which r is the radius of the nanotube plus the surfactant shell, t is the run time, μ is the fluid viscosity, G is the applied acceleration, and γ is $\ln(L/r)$ where L is the average length of the nanotubes. Using reasonable and known values, $L = 400$ nm, $\mu = 1.7$ mPa s, $t = 3240$ s (accounts for reduced rotational speed during acceleration and deceleration) and $G = 3.85 \times 10^6$ m/s^2 in eq 1, the density difference is on the order of 50 kg/m^3 ($r = 3$ nm). The literature value based on numerical simulations[23] is approximately 50−60 kg/m^3 for laser ablation diameter nanotubes, depending on whether the surfactant was allowed to interpolate into the nanotube. Although the values are consistent, the resolution of eq 1 is not sufficient to address whether the nanotubes ingest the surfactant. In the future we plan to investigate these samples using analytical ultracentrifugation to generate a more precise experimental value for the density difference.

Lastly, incorporating laser ablation and electric arc synthesized nanotubes into specific applications will likely require separation into highly enriched metallic and semiconducting type populations. The separation of both the NREL F3 and F5 samples were pursued using the cosurfactant DGU strategy.[4,6] Separation of the two fractions was found to be substantially different when exposed to the same cosurfactant processing and separation conditions. A picture of the separation performed under different conditions is shown in Figure 7. F5 was found to separate in a facile manner into metallic and semiconducting fractions,[50] whereas F3 did not cleanly separate, and the band positions

were different, under several conditions. Absorbance spectra of the collected fractions are shown as Figure 7B. The cause of this difference is unclear, but appears to be beyond the direct effect of the difference in the average buoyancy visible from the DOC only experiments. Possible explanations could include dissimilarities in the packing of the cosurfactants on the nanotube surface due to differences in polarizability, or the hypothesis that differential ingestion of the cosurfactants by the nanotubes induces the buoyancy differences necessary to separate the metallic and semiconducting SWCNTs.[23] Additional work is planned on this topic. However, the peak locations and Raman RBM modes of a commercial metallic separated nanotube dispersion,[51] exchanged into DOC solution, were evaluated in addition to the separated bands generated in this work. These optical features were found to be identical in location to those of F5 (Supporting Information).

In conclusion, separation of laser ablation and electric arc synthesized SWCNTs into distinct populations of empty and water-filled nanotubes was accomplished *via* a rapid and facile centrifugation-based separation. The optical properties of these two fractions were then demonstrated to be distinctly affected by the state of the nanotube interior, with the peak locations in absorbance and fluorescence displaying red-shifts with the presence of water in the nanotube cavity, and a hardening of the Raman RBM modes. The presence of water in the nanotube cavity was also found to facilitate the separation of the nanotubes into subpopulations of metallic and semiconducting SWCNTs. Selectivity for the empty cavity and water-filled populations was observed for SC, SDBS, and DOC dispersed nanotubes, but was most efficient for DOC dispersions. In DOC dispersion, the average density difference between the empty and water-filled laser ablation synthesis nanotubes was estimated as approximately 50 kg/m^3 providing a comparison for further development of computational experiments. By improving the understanding of selectivity for larger diameter nanotubes and isolating potential causes of experimental variation, we believe that the separation and study of empty and water-filled SWCNTs will be an important factor in developing nanotube applications.

METHODS

Dispersion of SWCNT soots was performed using sonication with sodium deoxycholate surfactant as previously reported.[30] Large aggregates, and most heavy impurities were subsequently removed through centrifugation for 2 h in a Beckman JA-20 rotor at 1885 Rad/s, retaining the supernatant. Absorbance spectra for purified but unsorted SWCNT dispersions show sharp features demonstrating effective dispersion (see Supporting Information). Separation at high applied centrifugation was performed in a Beckman VTi 65.2 rotor at 6806 rad/s ($\sim 4 \times 10^6$ m/s^2 radial acceleration) for 1 h; deceleration adds approximately 17 min, but at rapidly reduced acceleration. A two-step density gradient was used for the separation, a 1 mL bottom layer of either 15% or 18% (mass/volume) iodixanol (sold as OptiPrep, Aldrich) and 2% DOC, a 3 mL middle layer of 9% iodixanol, 1% DOC, and a top layer (0.9 mL) containing the SWCNT solution in 2% DOC. A 9% middle layer was initially chosen to closely approximate the average density, $\sim$1055 kg/m^3, measured for (6,5) nanotubes[4,31] in cholate surfactants. Postseparation, samples from multiple tubes/runs were collected, concentrated using membrane filtration, and dialyzed to remove all iodixanol prior to optical characterization.

UV−vis−NIR experiments were made in transmission geometry on a PerkinElmer Lambda 950 UV−vis-NIR spectrophotometer over a wavelength range of 2500−185 nm. The incident light was circularly polarized prior to the sample compartment, and the spectra were corrected for both dark current and background. The optical absorption spectra were recorded at 1 nm increments with an instrument integration time of at least 0.16 s per increment using a 1 mm path length quartz cuvette. The reference beam was left unobstructed, and the subtraction of the appropriate reference sample was performed during data reduction.

Photoluminescence excitation (PLE) contour maps were measured with a customized thermo-electron FT960 Raman spectrometer equipped with a Ge detector operating at 77 K. The excitation source was a 250 W tungsten-halogen bulb coupled to a single-grating monochromator, and the excitation intensity was <1 mW.[52] Samples were excited in 1 cm cuvettes in a front face configuration at an angle of $\sim$60°. All spectra were corrected for intensity variations in the lamp spectrum as well as for the responses of the system and detector.

The spontaneous Raman backscattered light was collected in a collinear 180° backscattering configuration with a triple grating spectrometer (Dilor XY800) and a liquid nitrogen cooled CCD detector. An Ar+ laser (Coherent Innova Sabre with multiline visible head) provided the (457.9, 488, and 514.5) nm excitation; in each case approximately 20 mW of power was focused to a spot size of approximately 100 μm within the liquid sample volume. The Ar+ laser was also used to pump a tunable wavelength TiSaph laser for wavelengths longer than 690 nm. A HeNe laser was used to provide the excitation at 632.8 nm. Cyclohexane was used selectively as a reference standard to ensure wavenumber accuracy.

Electronic-type separation was performed in a Beckman-Coulter SW-32 rotor for 19.25 h at 3350 rad/s and 20 °C. The solution layers for electronic separation were as follows (from bottom): 1 mL of 40% (mass per volume) iodixanol, 0.75% sodium dodecylsulfate (SDS), 0.75% sodium cholate; 2 mL of purified SWCNTs in 32% iodixanol, 1.125% SDS, 0.5% DOC; 20 mL of 30% mass per volume iodixanol, 1.125% SDS, and 1.125% SC. The laser SWCNT dispersion used in the separation was allowed to equilibrate in the mixed-surfactant environment for at least 4 days prior to separation. After separation, metallic and semiconducting fractions were collected and dialyzed repeatedly *via* forced filtration against a 30 kD membrane to exchange the SWCNTs into 1% DOC and to increase the absolute SWCNT concentration. Other conditions, including experiments with the top layer containing either 28% or 32% displayed similar degrees of separation for both F3 and F5 fractions, although the exact position of the layers after separation was lower and higher in the liquid columns, respectively, in those experiments.

Where reported, in data original to this contribution, the uncertainty is denoted by error bars equivalent to one standard deviation.

Acknowledgment. J. Blackburn, J. Holt, and B. Larsen were supported by the Solar Photochemistry program of the U.S. Department of Energy, Office of Science, Basic Energy Sciences, Division of Chemical Sciences, Geosciences and Biosciences, under Contract No. DE-AC36-08GO28308 to NREL.

Supporting Information Available: Detailed experimental procedures and additional optical characterization data on

the parent and separated fractions. This material is available free of charge *via* the Internet at http://pubs.acs.org.

REFERENCES AND NOTES

1. Liu, J.; Hersam, M. C. Recent Developments in Carbon Nanotube Sorting and Selective Growth. *MRS Bull.* **2010,** *35*, 315.
2. Fagan, J. A.; Bauer, B. J.; Hobbie, E. K.; Becker, M. L.; Hight Walker, A. R.; Simpson, J. R.; Chun, J.; Obrzut, J.; Bajpai, V.; Phelan, F. R.; *et al*. Carbon Nanotubes: Measuring Dispersion and Length. *Adv. Mater.* **2011,** *23*, 338–348.
3. Arnold, M. S.; Stupp, S. I.; Hersam, M. C. Enrichment of Single-Walled Carbon Nanotubes by Diameter in Density Gradients. *Nano Lett.* **2005,** *5*, 713.
4. Arnold, M. S.; Green, A. A.; Hulvat, J. F.; Stupp, S. I.; Hersam, M. C. Sorting Carbon Nanotubes by Electronic Structure Using Density Differentiation. *Nat. Nanotechnol.* **2006,** *1*, 60–65.
5. Ghosh, S.; Bachilo, S. M.; Weisman, R. B. Advanced Sorting of Single-Walled Carbon Nanotubes by Nonlinear Density-Gradient Ultracentrifugation. *Nat. Nanotechnol.* **2010,** *5*, 443–450.
6. Yanagi, K.; Miyata, Y.; Kataura, H. Optical and Conductive Characteristics of Metallic Single-Wall Carbon Nanotubes with Three Basic Colors; Cyan, Magenta, and Yellow. *Appl. Phys. Express* **2008,** *1*, 034003.
7. Green, A. A.; Hersam, M. C. Colored Semitransparent Conductive Coatings Consisting of Monodisperse Metallic Single-Walled Carbon Nanotubes. *Nano Lett.* **2008,** *8*, 1418–1422.
8. Niyogi, S.; Densmore, C. G.; Doorn, S. K. Electrolyte Tuning of Surfactant Interfacial Behavior for Enhanced Density-Based Separations of Single-Walled Carbon Nanotubes. *J. Am. Chem. Soc.* **2009,** *131*, 1144–1153.
9. Hároz, E. H.; Rice, W. D.; Lu, B. Y.; Ghosh, S.; Hauge, R. H.; Weisman, R. B.; Doorn, S. K.; Kono, J. Enrichment of Armchair Carbon Nanotubes *via* Density Gradient Ultracentrifugation: Raman Spectroscopy Evidence. *ACS Nano* **2010,** *4*, 1955–1962.
10. Nish, A.; Hwang, J.; Doig, J.; Nicholas, R. J. Highly Selective Dispersion of Single-Walled Carbon Nanotubes Using Aromatic Polymers. *Nat. Nanotechnol.* **2007,** *2*, 640–646.
11. Peng, X.; Komatsu, N.; Kimura, T.; Osuka, A. Simultaneous Enrichments of Optical Purity and (*n*,*m*) Abundance of SWNTs through Extraction with 3,6-Carbazolylene-Bridged Chiral Diporphyrin Nanotweezers. *ACS Nano* **2008,** *2*, 2045–2050.
12. Green, A. A.; Duch, M. C.; Hersam, M. C. Isolation of Single-Walled Carbon Nanotube Enantiomers by Density Differentiation. *Nano Res.* **2009,** *2*, 69.
13. Zheng, M.; Jagota, A.; Semke, E. D.; Diner, B. A.; McLean, R. S.; Lustig, S. R.; Richardson, R. E.; Tassi, N. G. DNA-Assisted Dispersion and Separation of Carbon Nanotubes. *Nat. Mater.* **2003,** *2*, 338.
14. Tu, X.; Manohar, A.; Jagota, A.; Zheng, M. DNA Sequence Motifs for Structure Specific Recognition and Separation of Carbon Nanotubes. *Nature* **2009,** *460*, 250–253.
15. Bonaccorso, F.; Hasan, T.; Tan, P. H.; Sciascia, C.; Privitera, G.; Di Marco, G.; Gucciardi, P. G.; Ferrari, A. C. Density Gradient Ultracentrifugation of Nanotubes: Interplay of Bundling and Surfactants Encapsulation. *J. Phys. Chem. C* **2010,** *114*, 17267–17285.
16. Green, M. J.; Young, C. C.; Parra-Vasquez, N. G.; Majumder, M.; Juloori, V.; Behabtu, N.; Pint, C. L.; Schmidt, J.; Kesselman, E.; Hauge, R. H.; *et al*. Direct Imaging of Carbon Nanotubes Spontaneously Filled with Solvent. *ChemComm.* **2011,** *47*, 1228–1230.
17. Sloan, J.; Hammer, J.; Zwiefka-Sibley, M.; Green, M. L. H. The Opening and Filling of Single Walled Carbon Nanotubes (SWTs). *Chem. Commun.* **1998,** 347–348.
18. Takenobu, T.; Takano, T.; Shiraishi, M.; Murakami, Y.; Ata, M.; Kataura, H.; Achiba, Y.; Iwasa, Y. Stable and Controlled Amphoteric Doping by Encapsulation of Organic Molecules inside Carbon Nanotubes. *Nat. Mater.* **2003,** *2*, 683–688.
19. Yanagi, K.; Miyata, Y.; Kataura, H. Highly Stabilized β-Carotene in Carbon Nanotubes. *Adv. Mater.* **2006,** *18*, 437–441.
20. Okubo, S.; Okazaki, T.; Hirose-Takai, K.; Suenaga, K.; Okada, S.; Bandow, S.; Iijima, S. Electronic Structures of Single-Walled Carbon Nanotubes Encapsulating Ellipsoidal C70. *J. Am. Chem. Soc.* **2010,** *132*, 15252–15258.
21. Hennrich, F.; Arnold, K.; Lebedkin, S.; Quintillá, A.; Wenzel1, W.; Kappes, M. M. Diameter Sorting of Carbon Nanotubes by Gradient Centrifugation: Role of Endohedral Water. *Phys. Stat. Sol., b* **2007,** *244*, 3896–3900.
22. Quintillá, A.; Hennrich, F.; Lebedkin, S.; Kappes, M. M.; Wenzel, W. Influence of Endohedral Water on Diameter Sorting of Single-Walled Carbon Nanotubes by Density Gradient Centrifugation. *Phys. Chem. Chem. Phys.* **2010,** *12*, 902–908.
23. Carvalho, E. J. F.; dos Santos, M. C. Role of Surfactants in Carbon Nanotubes Density Gradient Separation. *ACS Nano* **2010,** *4*, 765–770.
24. Wenseleers, W.; Cambré, S.; Čulin, J.; Bouwen, A.; Goovaerts, E. Effect of Water Filling on the Electronic and Vibrational Resonances of Carbon Nanotubes: Characterizing Tube Opening by Raman Spectroscopy. *Adv. Mater.* **2007,** *19*, 2274–2278.
25. Cambré, S.; Schoeters, B.; Luyckx, S.; Goovaerts, E.; Wenseleers, W. Experimental Observation of Single-File Water Filling of Thin Single-Wall Carbon Nanotubes Down to Chiral Index (5,3). *Phys. Rev. Lett.* **2010,** *104*, 207401.
26. Wenseleers, W. This research group presented independently gathered results showing empty and water-filled separation in a manner different from that related in this contribution at Nanotubes 2010 in Montreal. During this paper's revision, their in-press results were published online in ref 27.
27. Cambré, S.; Wenseleers, W. Separation and Diameter-Sorting of Empty (End-Capped) and Water-Filled (Open) Carbon Nanotubes by Density Gradient Ultracentrifugation. *Angew. Chem., Int. Ed.* **2011,** *50*, 2764–2768.
28. Wenseleers, W.; Vlasov, I. I.; Goovaerts, E.; Obraztsova, E.; Lobach, A. S.; Bouwen, A. Efficient Isolation and Solubilization of Pristine Single-Walled Nanotubes in Bile Salt Micelles. *Adv. Funct. Mater.* **2004,** *14*, 1105–1112.
29. Haggenmueller, R.; Rahatekar, S. S.; Fagan, J. A.; Chun, J.; Becker, M. L.; Naik, R. R.; Krauss, T.; Carlson, L.; Kadla, J. F.; Trulove, P. C.; *et al*. Comparison of the Quality of Aqueous Dispersions of Single Wall Carbon Nanotubes Using Surfactants and Biomolecules. *Langmuir* **2008,** *24*, 5070.
30. Fagan, J. A.; Becker, M. L.; Chun, J.; Nie, P.; Bauer, B. J.; Simpson, J. R.; Walker, A.R. H.; Hobbie, E. K. Centrifugal Length Separation of Carbon Nanotubes. *Langmuir* **2008,** *24*, 13880.
31. Fagan, J. A.; Becker, M. L.; Chun, J.; Hobbie, E. K. Length Fractionation of Carbon Nanotubes Using Centrifugation. *Adv. Mater.* **2008,** *20*, 1609.
32. *Centrifuges, Rotors, Tubes & Accessories Guide BR-8101L*; Beckman Coulter: Brea, CA, 2004; pp 1−23
33. Certain equipment, instruments or materials are identified in this paper in order to adequately specify the experimental details. Such identification does not imply recommendation by the National Institute of Standards and Technology nor does it imply the materials are necessarily the best available for the purpose.
34. Luton, P.; Ridgeway, G. L. Use of the Ultracentrifuge Vertical Rotor in the Detection of Rubella-Specific IgM on a Sucrose Density Gradient. *J. Clin. Path.* **1979,** *32*, 931–934.
35. Choi, J. H.; Strano, M. S. Solvatochromism in single-walled carbon nanotubes. *Appl. Phys. Lett.* **2007,** *90*, 22314.
36. Qian, H; Araujo, P. T.; Georgi, C.; Gokus, T.; Hartmann, N.; Green, A. A.; *et al.* Visualizing the Local Optical Response of Semiconducting Carbon Nanotubes to DNA-Wrapping. *Nano Lett.* **2008,** *8*, 2706–11.
37. Simpson, J. R.; Fagan, J. A.; Becker, M. L.; Hobbie, E. K.; Hight Walker, A. R. The Effect of Dispersant on Defects in Length-Separated Single-Wall Carbon Nanotubes Measured by Raman Spectroscopy. *Carbon* **2009,** *47*, 3238.

38. O'Connell, M. J.; Bachilo, S. M.; Huffman, C. B.; Moore, V. M.; Strano, M. S.; Haroz, E. H.; Rialon, K. L.; Boul, P. J.; Noon, W. H.; Kittrell, C.; *et al.* Band-Gap Fluorescence from Individual Single-Walled Carbon Nanotubes. *Science* **2002,** *297*, 593–596.
39. Bachilo, S. M.; Strano, M. S.; Kittrell, C.; Hauge, R. H.; Smalley, R. E.; Weisman, R. B. Structure-Assigned Optical Spectra of Single-Walled Carbon Nanotubes. *Science* **2002,** *298*, 2361–2366.
40. Weisman, R. B.; Bachilo, S. M. Dependence of Optical Transition Energies on Structure for Single-Walled Carbon Nanotubes in Aqueous Suspension: An Empirical Kataura Plot. *Nano Lett.* **2003,** *3*, 1235–1238.
41. Tsyboulski, D. A.; Bakota, E. L.; Witus, L. S.; Rocha, J. R.; Hartgerink, J. D.; Weisman, R. B. Self-Assembling Peptide Coatings Designed for Highly Luminescent Suspension of Single-Walled Carbon Nanotubes. *J. Am. Chem. Soc.* **2008,** *130*, 17134–17140.
42. Blackburn, J. L.; McDonald, T. J.; Metzger, W. K.; Engtrakul, C.; Rumbles, G.; Heben, M. J. Protonation Effects on the Branching Ratio in Photoexcited Single-Walled Nanotube Dispersions. *Nano Lett.* **2008,** *8*, 1047.
43. Ju, S.; Kopcha, W. P.; Papadimitrakopoulos, F. Brightly Fluorescent Single-Walled Carbon Nanotubes *via* an Oxygen-Excluding Surfactant Organization. *Science* **2009,** *323*, 1319.
44. Nugraha, A. R. T.; Saito, R.; Sato, K.; Araujo, P. T.; Jorio, A.; Dresselhaus, M. S. Dielectric constant model for environmental effects on the exciton energies of single wall carbon nanotubes. *Appl. Phys. Lett.* **2010,** *97*, 091905.
45. Sato, K.; Saito, R.; Nugraha, A. R. T.; Maruyama, S. Excitonic Effects on Radial Breathing Mode Intensity of Single Wall Carbon Nanotubes. *Chem. Phys. Lett.* **2010,** *497*, 94.
46. Jorio, A.; Fantini, C.; Pimenta, M. A.; Capaz, R. B.; Samsonidze, Ge. G.; Dresselhaus, G.; Dresselhaus, M. S.; Jiang, J.; Kobayashi, N.; Grüneis, A.; Saito, R. Resonance Raman Spectroscopy (*n*,*m*)-Dependent Effects in Small-Diameter Single-Wall Carbon Nanotubes. *Phys. Rev. B* **2005,** *71*, 075401.
47. Maultzsch, J.; Telg, H.; Reich, S.; Thomsen, C. Radial Breathing Mode of Single-Walled Carbon Nanotubes: Optical Transition Energies and Chiral-Index Assignment. *Phys. Rev. B* **2005,** *72*, 205438.
48. Araujo, P. T.; Maciel, I. O.; Pesce, P. B. C.; Pimenta, M. A.; Doorn, S. K.; Qian, H.; Hartschuh, A.; Steiner, M.; Grigorian, L.; Hata, K.; *et al.* Nature of the Constant Factor in the Relation between Radial Breathing Mode Frequency and Tube Diameter for Single-Wall Carbon Nanotubes. *Phys. Rev. B.* **2008,** *77*, 241403.
49. Lu, Q.; Keskar, G.; Ciocan, R.; Rao, R.; Mathur, R. B.; Rao, A. P.; Larcom, L. L. Determination of Carbon Nanotube Density by Gradient Sedimentation. *J. Phys. Chem. B* **2006,** *110*, 24371–24376.
50. Hobbie, E. K.; Fagan, J. A.; Obrzut, J.; Hudson, S. D. Microscale Polymer−Nanotube Composites. *Appl. Mater. Int.* **2009,** *1*, 1561–1566.
51. Nanointegris 98% metallic nanotubes, dispersed, batch M10-744, 99% semiconductng batch S10-671.
52. McDonald, T. J.; Jones, M.; Engtrakul, C.; Ellingson, R. J.; Rumbles, G.; Heben, M. J. Near-Infrared Fourier Transform Photoluminescence Spectrometer with Tunable Excitation for the Study of Single-Walled Carbon Nanotubes. *Rev. Sci. Instrum.* **2006,** *77*, 053104.